



## Numerical Investigation of Joint Shear Strength of Circular CFST Column Connected to Steel I-Beam with External Diaphragm

S. Sivraj<sup>1\*</sup>, Deepak Yadav<sup>2</sup>, Dipti Ranjan Sahoo<sup>3</sup> and Ashok Gupta<sup>4</sup>

<sup>1</sup>PhD Student, Department of Civil Engineering, IIT Delhi – New Delhi, India

<sup>2</sup>Post-doctoral Fellow, Department of Civil Engineering, IIT Delhi – New Delhi, India

<sup>3</sup>Professor, Department of Civil Engineering, IIT Delhi – New Delhi, India

<sup>4</sup>Former Professor, Department of Civil Engineering, IIT Delhi – New Delhi, India

\*[sivraj.eq@gmail.com](mailto:sivraj.eq@gmail.com) (Corresponding Author)

### ABSTRACT

This study presents the numerical study of steel I-beam to circular CFST column assemblies with the external diaphragm to investigate the panel zone seismic performance. The finite element model is developed, and the model's validity is verified by comparing the numerical results with the experimental data from previous literature. A parametric study has been conducted to investigate the cyclic behavior of beam-column joints. The key parameters varied in the present study are the panel zone aspect ratio, the width-to-thickness ratio of the tube, and the axial load ratio of the CFST column. To study the shear capacity of the panel zone, a weak panel zone was taken explicitly into account in all the specimens. The joint shear strength obtained numerically has been compared with the design code AIJ (1987), Eurocode (2005), and other methods proposed in the previous literature. Results show that the joint shear strength equations need refinement to accurately predict the panel zone behavior. The impact of considered parameters on joint shear strength and cyclic behavior has been presented.

Keywords: Concrete Filled Steel Tube (CFST), Beam-Column Joint, Panel Zone, Numerical Modelling, Joint Shear Strength.

### INTRODUCTION

Concrete-filled steel tube (CFST) columns have become more popular in structural applications [1]. CFST columns are advantageous in a high-rise building that demands high strength and large functional space. Axial strength can be enhanced with the use of a CFST column as compared to bare steel or bare reinforced concrete columns. CFST column combines the advantages of steel and concrete; steel acts as a casing and provides confinement to the concrete, thus improving ductility. Concrete provides stiffness and prevents or delays the steel tube's local buckling [2], [3].

Kloppel and Goder were the first to study the CFST columns [4]. Since then, many researchers have performed tests to investigate the axial strength of CFST members [5]–[7]. The application of CFST columns attracted the attention of researchers after the Great Kanto Earthquake in 1923 [8], as existing composite structures were found to be relatively undamaged in this earthquake. Since then many buildings of over five stories in Japan have been framed with composite steel-concrete columns, according to Wakabayashi [9]. In Seattle, Washington, several structures were constructed in the mid-1980s that became well-known for their use of CFST columns. These high-rise buildings used CFST as the primary lateral load-resistant system [3]. Some examples of CFST members in practical applications are SEG Plaza Shenzhen, China, Wuhan International Securities Building, and a few other buildings and bridges as described by Zhao et al. [10].

Despite having many benefits, the use of CFST in building construction has been constrained due to factors such as insufficient construction experience, limited comprehension of design provisions, and the complexity of connection details. Many well-known national codes provide guidelines for the CFST structures, such as the Japanese code AIJ-1997 [11], American code AISC [12], British bridge code BS5400 [13], Chinese code DBJ13-51 [14], Australian bridge code AS5100 [15] and Eurocode 4 [16]. With extensive research on the flexural and axial behavior of the CFST members in the past, these standards provide sufficient guidelines for designing flexural and axial members. However, relatively less information is available on the behavior of the joints, which hold a significant role in determining whether a building structure can reach its theoretical ultimate load since plastic hinges are typically formed at the location of two or more members [17].

A traditional moment-resisting connection, which comprises a steel beam and a CFST column, is extensively employed in tall buildings and has been extensively investigated by numerous scholars [18]. The connection configuration between a concrete-filled steel tube (CFST) column and a steel beam can be categorized into three types: internal diaphragm connection, through diaphragm connection, and external diaphragm connection. Understanding the shear deformation behavior of these connections has become crucial to evaluate the seismic performance and design of these structures. Previous researchers have proposed several empirical methods to predict the panel zone shear force and deformation [19], [20]. However, very few experimental studies address the joint shear-deformation behavior of CFST columns and steel beam joints. Empirical equations from previous studies cannot predict the skeleton curves accurately over a wide range of geometric parameters such as joint aspect ratio, width-to-thickness ratio, and axial load ratio under the effect of repetitive cyclic loading, which is very common in seismic events.

This study is focused on addressing the issue of prediction of joint shear-deformation over a wide range of practical geometric parameters. A parametric study has been conducted on finite element software by varying the geometric parameters and axial load ratio. The first numerical analysis procedure is validated against experimental findings by previous researchers [17], [21]. A validated numerical analysis procedure has been used to model the specimens for parametric study and formulate the empirical equations of joint shear-deformation skeleton curves.

### SCOPE AND OBJECTIVE

In this research, an interior connection comprising a steel beam and circular CFST column has been considered for the study. Panel zone behavior has been investigated by modeling a beam-column joint sub-assembly numerically in a finite element analysis software ABAQUS [22]. The objectives of this study are to investigate the joint shear-deformation behavior of the CFST column and steel beam joint. To conduct the parametric study for studying the effects of axial load ratio, joint aspect ratio, and width-to-thickness ratio on joint shear-deformation behavior. To evaluate the skeleton curves of joint shear-deformation and propose the empirical equations based on the numerical results from the parametric study.

### CFST COLUMN TO STEEL BEAM CONNECTION DETAILS

This study considers a circular CFST column connected to an I-shaped steel beam with an external diaphragm. The geometric description of the considered beam-column sub-assembly is shown in Figure 1. As the point of inflection in beams and columns is approximately assumed to be at their mid-lengths, the bottom end of the column is pinned, the vertical deflection of the beam ends is constrained, and lateral cyclic loads are applied at the column's top end. The variable specifications of the specimen are steel tube thickness ( $t$ ), panel zone tube thickness ( $t_s$ ), overall depth of the beam ( $h$ ), and applied axial load on the column top ( $N$ ). Other specifications that are kept constant in all specimens are shown in Figure 1.

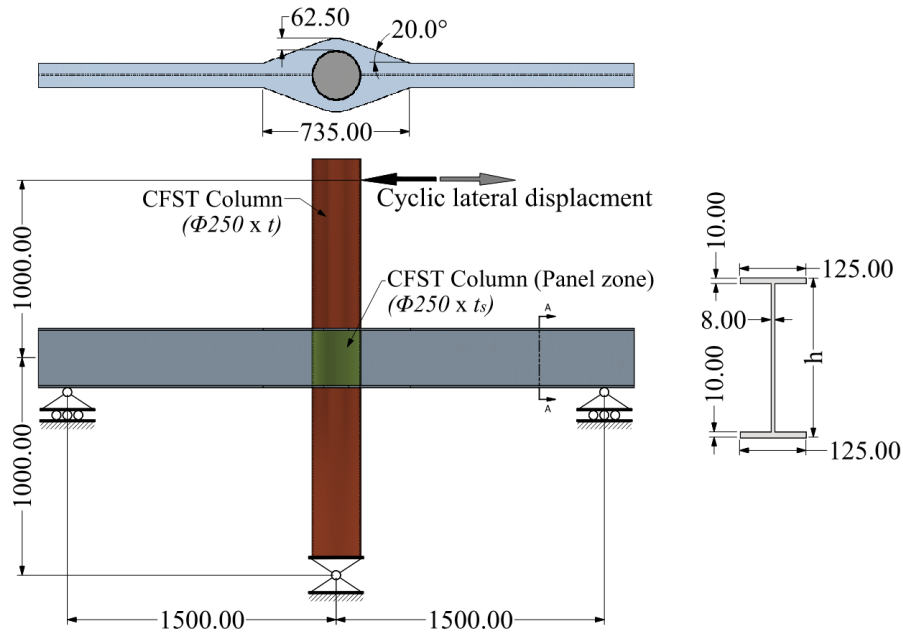


Figure 1. Connection configuration (Unit: mm)

## FINITE ELEMENT MODELING

### General descriptions

Finite element analysis software ABAQUS [22] is used to model beam-column joint sub-assembly with circular CFST column to I-shaped steel beam under lateral cyclic load applied at the column top end. For an accurate simulation of the behavior of the beam-column joint sub-assembly, it is necessary to model the five main components. These components include the confined concrete, steel tube, steel beam, the interface and contact between the concrete and steel tube, and the connection between steel tube and steel beam. Apart from these parameters, it is also essential to consider the proper selection of element type, mesh size, boundary conditions, and load applications to ensure precise and reasonable results in simulating the behavior of the beam-column joint [23]. The numerical modeling approach adopted for this study has been described in subsequent sections. Then the results are validated against the two experimental results presented by Wang et al. [17] and Zhang et al. [21].

### Finite element type

Figure 2 shows the components of the beam-column joint model, i.e., steel tube, steel beam, and concrete infill. Eight-node solid elements (C3D8R) with reduced integration are utilized to model the infill concrete. The steel tube and beam are modeled using a four-node shell element (S4R) with reduced integration [24], [25]. Due to their high length-to-thickness ratio, the steel tube and beam are considered thin and are thus modeled as shell elements.

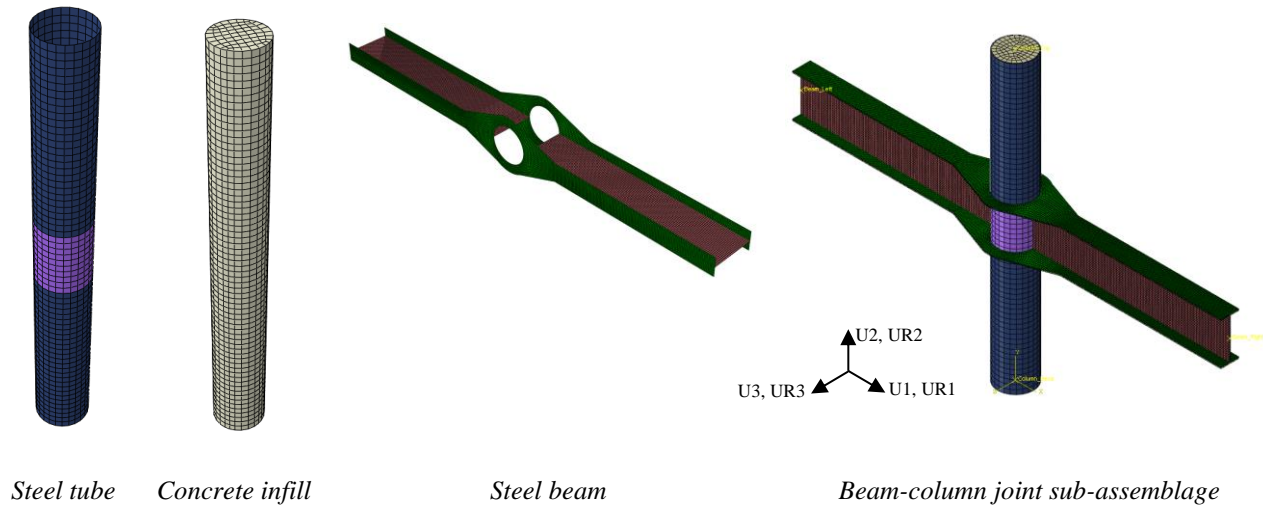


Figure 2. Finite element modeling of various components of beam-column joint

### Constraint and interaction properties

The welded connection between the steel beam and steel tube is simulated using the tie constraint, which effectively binds the two separate surfaces together to prevent relative motion between them. To model the interaction between the steel tube and concrete infill, surface-to-surface contact was adopted in the current simulation. Hard contact was assigned in the normal direction, and friction was assigned in the tangential direction. Past studies have used a coefficient of friction ranging from 0.25 to 0.6 [3], [26]. A coefficient of friction of 0.6 was chosen for the present study, which is in agreement with the majority of experimental results [27].

### Initial boundary conditions and loading

The free end surface of the beam and column are coupled to a reference point, and boundary conditions are applied to these reference points. The bottom end of the column was assigned pinned boundary condition (i.e.,  $U_1=U_2=U_3=UR_1=UR_2=0$ ,  $UR_3 \neq 0$ ), the top column end was assigned pinned condition with allowed lateral and longitudinal movement (i.e.,  $U_3=UR_1=UR_2=0$ ,  $U_1 \neq 0$ ,  $U_2 \neq 0$ ,  $UR_3 \neq 0$ ), and the beam free end was assigned pinned with allowed longitudinal movement (i.e.,  $U_2=U_3=UR_1=UR_2=0$ ,  $U_1 \neq 0$ ,  $UR_3 \neq 0$ ). A constant axial compression load was applied to the column and maintained throughout the loading step. Subsequently, a cyclic lateral load was applied to the top end of the column. The loading history of the lateral load applied is illustrated in Figure 3.

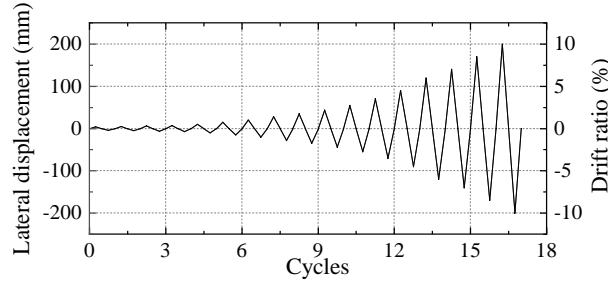


Figure 3. Imposed lateral displacement history.

### Concrete material model

For modeling concrete infill concrete damaged plasticity (CDP) constitutive model in ABAQUS [22] is utilized. A combination of non-associated multi-hardening plasticity and scalar damaged elasticity to describe the irreversible damage that occurs during the concrete damage process is adopted in the CDP model [21]. This method was developed initially by Lubliner et al. [28] and was later modified by Lee and Fenves [29]. The material parameters and their values considered in the analysis are the ratios of the second stress invariant on the tensile meridian to that on the compression meridian ( $K_c$ ) = 0.6667, dilation angle ( $\psi$ ) = 40°, flow potential eccentricity ( $e$ ) = 0.1, the ratio of initial equi-biaxial compressive yield stress to initial uniaxial compressive yield stress ( $\sigma_{b0}/\sigma_{c0}$ ) = 1.16, and the viscosity parameter ( $\mu$ ) = 0.001. Poisson's ratios of 0.2 and 0.3 were assumed in the present study for concrete and steel, respectively. Elastic modulus of concrete ( $E_c$ ) were computed using the empirical Eq. (1) recommended in ACI 318 [30], where  $f_c$  is in MPa. For the present study characteristics compressive strengths of cube ( $f_c$ ) is considered as 30 MPa.

$$E_c = 4700\sqrt{f_c} \quad (1)$$

A three-stage model recommended by Tao et al. [27] representing the strain hardening/softening rule of concrete confined by steel tubes, as shown in Figure 4(a), was utilized in this study.

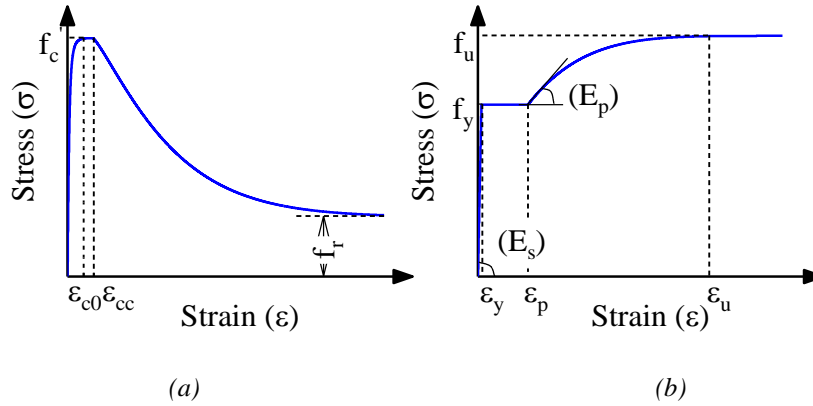


Figure 4. (a) Compression stress-strain model for concrete infill, (b) Stress-strain model for steel

The tensile behavior of concrete has been adopted from the recommendations given in Model Code 1990 [31]. Concrete brittle behavior is generally characterized by its stress-crack displacement response. At critical points, the strain over the characteristic length,  $l_c$  can be calculated from corresponding crack displacements as shown in Figure 5(a). In this study,  $l_c$  was defined as the size of the finite element in the concrete mesh. Eq. (2) was employed to compute the fracture energy,  $G_f$  for a maximum aggregate size of 16 mm. Damage parameters in compression and tension corresponding to strain values are shown in Figure 5(b) and Figure 5(c), respectively [32].

$$G_f = 0.030(0.1f_{cm})^{0.7} \quad (2)$$

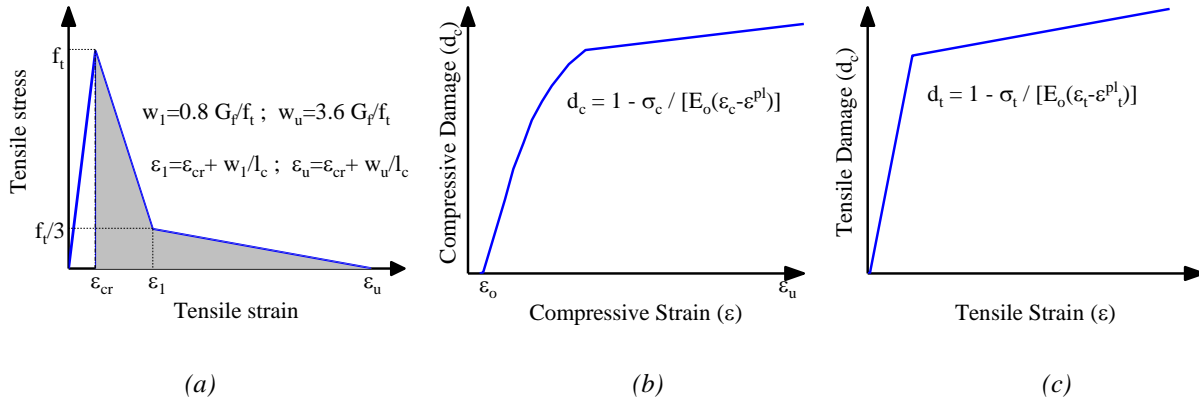


Figure 5. (a) Tensile stress-strain model for concrete infill, (b) Compression damage parameter-strain relationship for concrete, (c) Tensile damage parameter-strain relationship for concrete

### Steel material model

The stress-strain model recommended by Tao et al. [27] was used to model the steel material in a circular CFST column, as shown in Figure 4(b). In this study yield and ultimate strength of structural steel are considered as  $f_y = 350$  MPa and  $f_u = 490$  MPa, respectively.

### Numerical Validation

To validate the numerical modeling approach as described above, two experimental results presented by Wang et al., 2008 [17] and Zhang et al., 2012 [21] have been considered. In both the literature, the seismic performance of interior beam-column joint sub-assembly with external diaphragms has been experimentally studied. In an experiment conducted by Zhang et al., failure modes have been investigated by varying the axial load levels. A numerical analysis of specimen J-4 has been performed for validation of the current numerical modeling approach, and the force-deformation curve is compared as shown in Figure 6. The predicted initial stiffness is 7% and 10% higher under the positive and negative moment, respectively as compared with the experiment. The predicted ultimate capacity is 2% less than that of the experimental result.

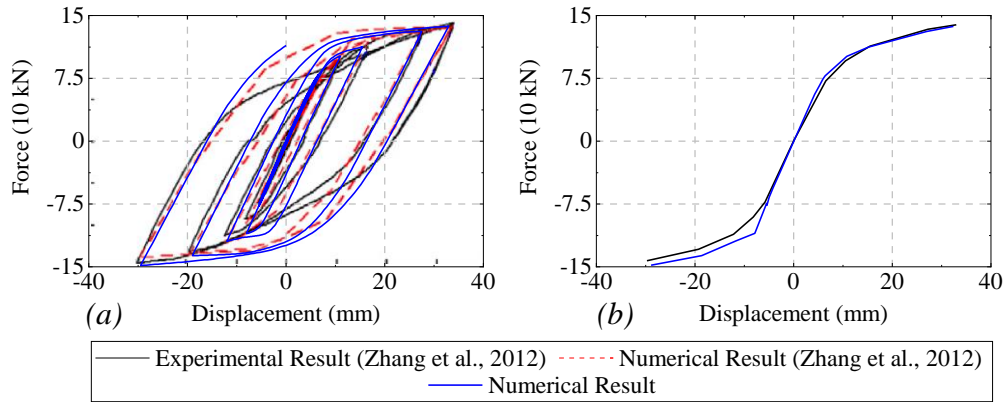


Figure 6. Comparison of numerical result and test (Specimen J-4) conducted by Zhang et al.[21] (a) Force-Displacement curve (b) Skeleton curve of force-displacement hysteretic curve.

In the experiment conducted by Wang et al., hysteretic behavior under combined constant axial load and cyclic lateral load have been investigated on beam-column joint subassembly with reduced beam section configured steel beam. A numerical analysis of the specimen CJ-22N has been performed and compared the numerical results with the experimental result as shown in Figure 7. The predicted initial stiffness is 4% and 6% higher under positive and negative moments, respectively as compared with the experiment. The predicted ultimate capacity is 4% less than that of the experimental result. With these observations, it is found that the modeling approach adopted for the present study as described in the above section, is in good agreement with the experimental results and can be used for a parametric study.

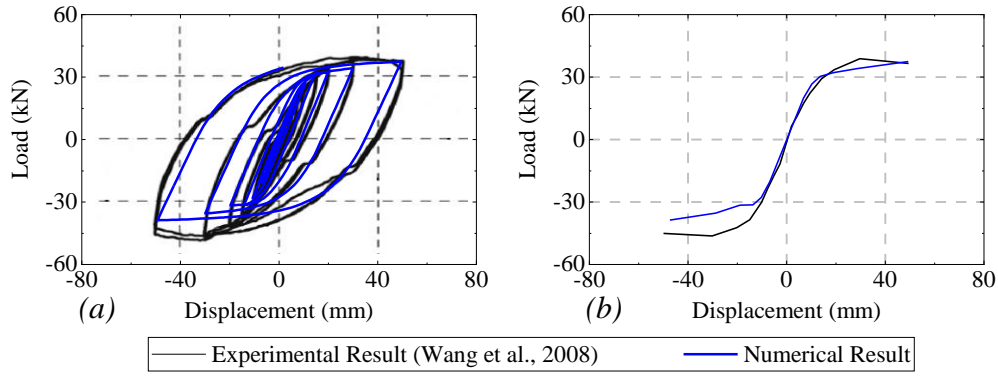


Figure 7. Comparison of numerical result and test (Specimen CJ-22N) conducted by Wang et al.[17] (a) Force-Displacement curve (b) Skeleton curve of force-displacement hysteretic curve.

## PARAMETRIC STUDY

### Specimen details

A total of 27 specimens were considered for the parametric study varying steel tube thickness ( $t$ ), panel zone tube thickness ( $t_s$ ), the overall depth of the beam ( $h$ ), and applied axial load on the column top ( $N$ ) as listed in Table 1. The parameters investigated in the study include: the panel zone aspect ratio ( $h/D = 0.7, 0.9, 1.2$ ), the width-to-thickness ratio of the tube ( $D/t_s = 62.5, 83.3, 125.0$ ), and the axial load ratio of the CFST column ( $N/N_0 = 0, 0.2, 0.4$ ). The axial capacity ( $N$ ) of CFST columns were computed as per AISC Standard [12]. External diaphragm-type connection is considered for the present study as shown in Figure 1, with a thickness the same as that of the beam flange. To ensure the shear failure of the joint occurs before the yielding of steel members, the tube thickness was reduced explicitly at the panel region [20]. The shear deformation of the specimens obtained numerically was then compared with the empirical methods proposed by previous researchers.

### Results and discussions

The specimens listed in Table 1 are modeled in ABAQUS [22] as described in the above section. Numerical analysis has been performed for all 27 specimens for the lateral cyclic load and the load-displacement hysteresis curve has been plotted. The skeleton curves of the load-displacement curve are then obtained by connecting the displacement peaks of all cycles. The joint shear force thus induced are calculated using the lateral force and shear deformation of the panel zone ( $\gamma$ ) have been estimated from the diagonal deformation as shown in Figure 8 using Eq. (3). From the plot, as shown in Figure 9(c), it is observed that as the axial load level increases the joint strength increases slightly. As the concrete core is under tri-axial compression due to the axial compression and the confining effect provided by the steel tube, that enhances the load-carrying capacity and inelastic deformation. The shear strength of the panel zone decreases as the aspect ratio increased as shown in Figure 9(b).

$$\gamma = \frac{\sqrt{h^2 + D^2}}{2 \cdot h \cdot D} (\Delta_1 - \Delta_2) \quad (3)$$

Figure 8 is a diagram illustrating the shear deformation of a panel zone. It shows a cross-section of a panel zone with height  $h$  and width  $D$ . The diagram shows the original shape (dashed lines) and the deformed shape (solid lines). The horizontal displacement of the top edge is labeled  $\Delta_1$  and the horizontal displacement of the bottom edge is labeled  $\Delta_2$ .

Figure 8. Shear deformation of panel zone.

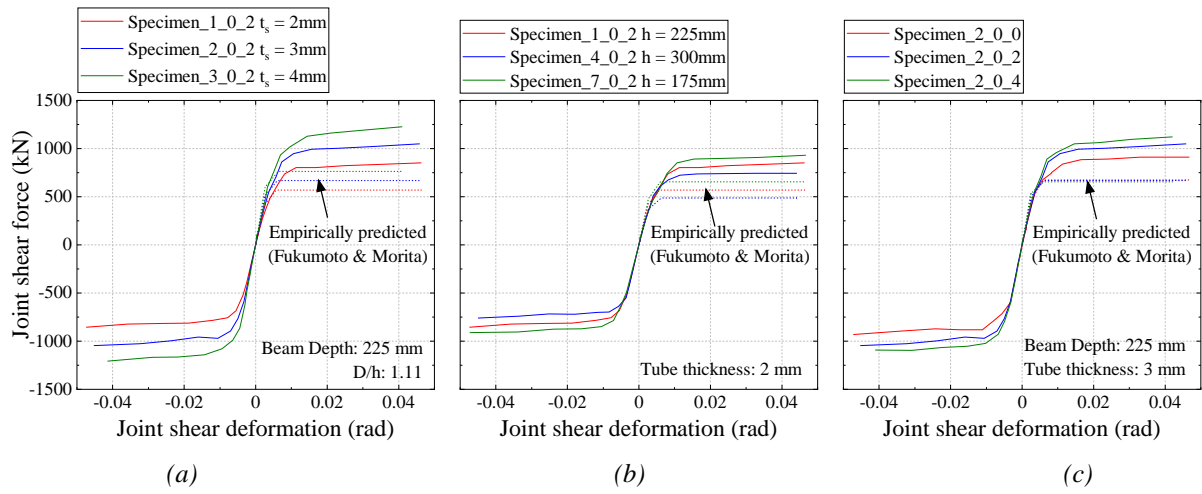


Figure 9. Skeleton curves of joint shear force vs. joint shear deformation curve

Table 1. Specimen details

Specimen name	Axial load ratio	Panel zone aspect ratio	Width-to-thickness ratio	Axial load applied	Tube thickness	Panel zone tube thickness	Beam overall depth
	$N/N_0$	$h/D$	$D/t_s$	$N$ (kN)	$t$	$t_s$	$h$
Specimen_1_0	0	0.90	125.0	0.0	3	2	225
Specimen_2_0			83.3	0.0	4	3	
Specimen_3_0			62.5	0.0	5	4	
Specimen_4_0	0.2	1.20	125.0	0.0	3	2	300
Specimen_5_0			83.3	0.0	4	3	
Specimen_6_0			62.5	0.0	5	4	
Specimen_7_0	0.70	0.70	125.0	0.0	3	2	175
Specimen_8_0			83.3	0.0	4	3	
Specimen_9_0			62.5	0.0	5	4	
Specimen_1_0.2	0.4	0.90	125.0	480.0	3	2	225
Specimen_2_0.2			83.3	527.5	4	3	
Specimen_3_0.2			62.5	575.0	5	4	
Specimen_4_0.2	0.4	1.20	125.0	480.0	3	2	300
Specimen_5_0.2			83.3	527.5	4	3	
Specimen_6_0.2			62.5	575.0	5	4	
Specimen_7_0.2	0.70	0.70	125.0	480.0	3	2	175
Specimen_8_0.2			83.3	527.5	4	3	
Specimen_9_0.2			62.5	575.0	5	4	
Specimen_1_0.4	0.4	0.90	125.0	960.0	3	2	225
Specimen_2_0.4			83.3	1055.0	4	3	
Specimen_3_0.4			62.5	1147.5	5	4	
Specimen_4_0.4	0.4	1.20	125.0	960.0	3	2	300
Specimen_5_0.4			83.3	1055.0	4	3	
Specimen_6_0.4			62.5	1147.5	5	4	
Specimen_7_0.4	0.70	0.70	125.0	960.0	3	2	175
Specimen_8_0.4			83.3	1055.0	4	3	
Specimen_9_0.4			62.5	1147.5	5	4	

The joint shear strength and deformation are then compared with previously proposed empirical methods [19], [20]. It is observed that the predicted shear strength is underestimated by the empirical equation proposed by Fukumoto and Morita [19] as shown in Figure 9. Fukumoto and Morita have proposed a shear strength and stiffness reduction ratio using regression formulations. The shear model proposed is not taken hardening into account, in this study a factor has been proposed to determine the slope of the third branch of the tri-linear model. Also, the multiple regression analysis has been performed to modify the formulations for the shear strength ratio ( $\beta$ ) and stiffness reduction ratio ( $\alpha_{cu}$ ).

### PROPOSED MODIFICATION IN MODEL

Fukumoto and Morita [19] have proposed a trilinear model having a yield strength point and an ultimate strength point for a panel zone as shown in Figure 10(a). In this study based on the numerical results the modification to the equation of the shear strength ratio ( $\beta$ ) and stiffness reduction ratio ( $\alpha_{cu}$ ) have been proposed and the hardening is taken into consideration in third branch of the tri-linear model as a function of axial load ratio, joint aspect ratio, or width-to-thickness ratio (Figure 10(b)).

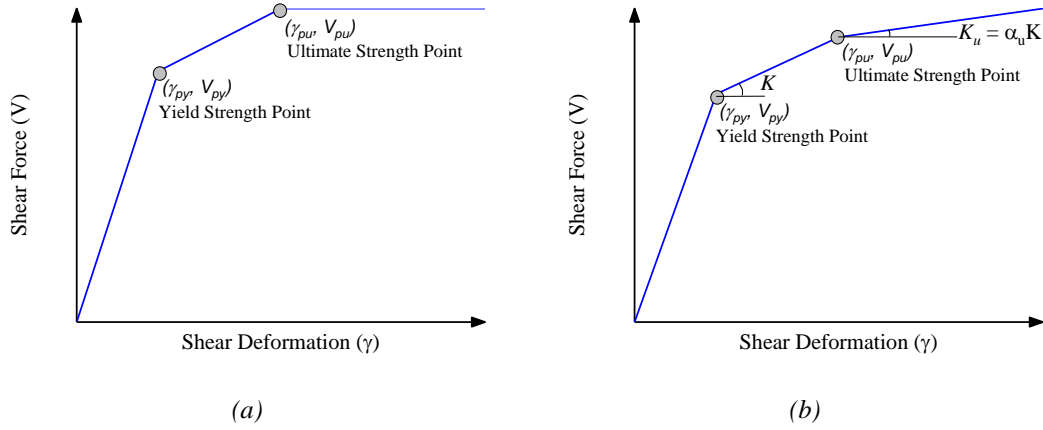


Figure 10. Shear force-deformation relation for panel zone (a) model proposed by Fukumoto and Morita [19] (b) proposed modified model

Multiple regression analysis was performed to predict the stiffness reduction ratio using axial load ratio and tube thickness to tube width ratio, as it was found that neither of these factors was closely associated with the stiffness reduction ratio (Figure 12). The resulting regression formula for  $\alpha_{cu}$  is derived from these factors and is presented in Eq. (4). The stiffness reduction ratio is employed to compute the deformation  $\gamma_{cu}$  corresponding to ultimate strength of the concrete core  $V_{cu}$ .

$$\alpha_{cu} = 0.07 + 0.10 \left( \frac{N}{N_0} \right)^{0.97} + 45.09 \left( \frac{t_s}{D} \right)^{1.8} \quad (4)$$

The shear yield to ultimate strength ratio ( $\beta = V_{cy}/V_{cu}$ ) computed from the numerical results were plotted with the corresponding axial load ratio and tube thickness to tube width ratio, as shown in Figure 11. Regression analysis was performed to predict the stiffness reduction ratio using the axial load ratio and tube thickness to tube width ratio. The resulting regression formula for  $\beta$  is derived from these factors and is presented in Eq. (5).

$$\beta = 0.64 + 0.38 \left( \frac{N}{N_0} \right)^{1.7} + 1.58 \left( \frac{t_s}{D} \right) \quad (5)$$

From the skeleton curve of the joint shear-deformation curve, it is observed that there is a slight slope in the shear-deformation curve which is not in agreement with the shear model proposed by Fukumoto and Morita. The ratio of stiffness at the ultimate point to stiffness at the yield point  $\alpha_u$  is employed to estimate the slope of the third branch of the tri-linear model. The variation of  $\alpha_u$  have been observed corresponding to different axial load ratio, width-to-thickness ratios, and aspect ratio of panel zone, and it is found that the variation of  $\alpha_u$  is closer to the width-to-thickness ratio of steel tube. The regression expression for  $\alpha_u$  is given in Eq. (6). Further, it should be noted that the present study has been performed maximum up to the shear deformation of 0.04 radians, for higher deformation further study must be done.

$$\alpha_u = 0.001 \left( \frac{t_s f_y}{D} \right)^{2.6} \quad (6)$$

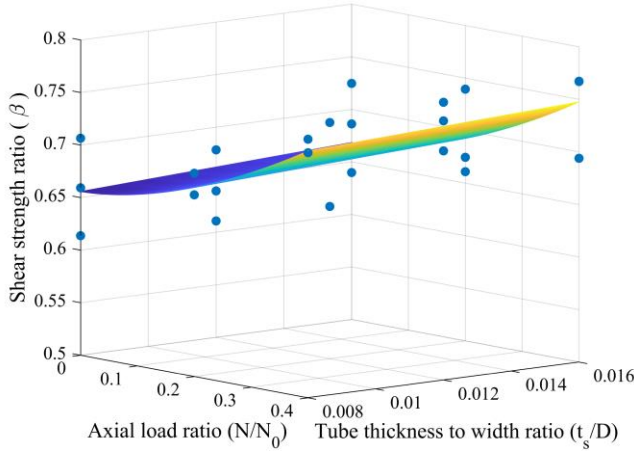


Figure 11. Shear strength ratio of yielding-to-ultimate vs. axial load ratio and tube thickness-to-width ratio

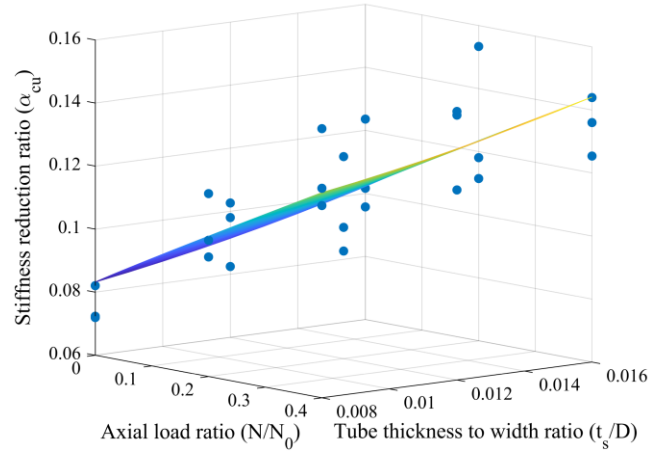


Figure 12. Stiffness reduction ratio vs. axial load ratio and tube thickness to width ratio

The joint shear-deformation curve obtained numerically and predicted by modified equations have been plotted as shown in Figure 13(a) for comparison. Further, the predicted yield and ultimate shear strength are plotted against the numerical results as shown in Figure 13(b), and Figure 13(c) respectively, it is observed that the predicted shear-deformation model is in good agreement with the numerical results.

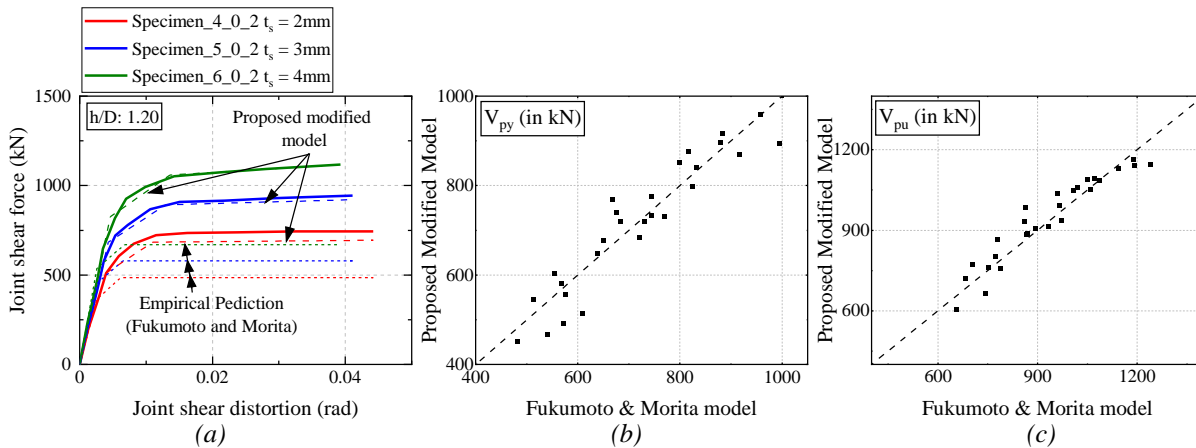


Figure 13. (a) Comparison of numerical results with empirical results estimated by Fukumoto and Morita model and proposed modified model (b) Comparison of predicted shear force at yield point with numerical result (c) Comparison of predicted shear force at ultimate point with numerical result.

## SUMMARY AND CONCLUSIONS

In this research, an interior connection comprising a steel beam and circular CFST column has been considered. A FEM modeling approach for a circular CFST column to steel beam has been discussed and the procedure is validated against the experimental results by previous researchers. A wide range of practical geometric parameters of the beam-column joint configuration is considered varying axial load ratio, joint aspect ratio, and width-to-thickness ratio. Numerical analysis has

been performed and joint shear-deformation behavior curves are compared with previous empirical prediction approaches, mainly focusing on Fukumoto and Morita [19] shear model. Observed that the prediction of shear-deformation is not in good agreement with the numerical results. Then the regression analysis has been performed to modify the expressions for the shear strength ratio ( $\beta$ ) and stiffness reduction ratio ( $\alpha_{cu}$ ). The shear-deformation was then computed using modified equations and compared with numerical results, and observed they are in good agreement with numerical results. Following conclusions have been drawn within the limitations of the present study:

- The FE modeling approach described in this paper predicted results that are in good agreement with the experimental findings of previous researchers [17], [21].
- For the interior circular CFST column to steel beam with external diaphragm configuration, as the concrete core is under tri-axial compression due to the axial compression and the confining effect provided by the steel tube. The axial load enhances the shear capacity of the panel zone.
- The third branch of the tri-linear backbone curve has been proposed considering hardening. The previous models did not take the hardening into account in their tri-linear shear model.

## REFERENCES

- [1] Han, L.H. (2002). “Tests on stub columns of concrete-filled RHS sections”. *Journal of Constructional Steel Research*, 58(3), pp. 353–372.
- [2] Furlong, R.W. (1968). “Design of Steel-Encased Concrete Beam-Columns”. *Journal of the Structural Division*, 94(1), pp. 267–281.
- [3] Schneider, S.P. (1998). “Axially Loaded Concrete-Filled Steel Tubes”. *Journal of Structural Engineering*, 124(10), pp. 1125–1138.
- [4] Kloppel, V.K., and Goder, W. (1957). “An investigation of the load carrying capacity of concrete-filled steel tubes and development of design formula”. *Der Stahlbau*, 1, pp. 1–10.
- [5] Furlong, R.W. (1967). “Strength of Steel-Encased Concrete Beam Columns”. *Journal of the Structural Division*, 93(5), pp. 113–124.
- [6] Fujimoto, T., Mukai, A., Nishiyama, I., and Sakino, K. (2004). “Behavior of Eccentrically Loaded Concrete-Filled Steel Tubular Columns”. *Journal of Structural Engineering*, 130(2), pp. 203–212.
- [7] Wei, J., Luo, X., Lai, Z., and Varma, A.H. (2020). “Experimental Behavior and Design of High-Strength Circular Concrete-Filled Steel Tube Short Columns”. *Journal of Structural Engineering*, 146(1).
- [8] Chen, W.F., and Liew, J.Y.R. (2002). *The Civil Engineering Handbook*. Second Edi. CRC Press.
- [9] Wakabayashi, M. (1991). “Introductory Remarks”. In *3rd International Conference of Steel-Composite Structures*, p. 15.
- [10] Zhao, X.-L., Han, L.-H. and Lu, H. (2010). *Concrete-filled Tubular Members and Connections*. CRC Press.
- [11] Architectural Institute of Japan (1997). *Recommendations for design and construction of concrete filled steel tubular structures*. Japan.
- [12] AISC, 360-16 (2016). *Specification for Structural Steel Buildings*. American Institute of Steel Construction, Chicago, Illinois, USA.
- [13] British standard Institution (2005). *BS 5400 Steel, concrete and composite bridges, Part 5, Code of practice for the design of composite bridges*. British standard Institution, London UK.
- [14] DBJ 13-51-2003 (2003). *Technical specification for concrete-filled steel tubular structures*. The Construction department of Fujian province, Fuzhou, China [Preprint].
- [15] Standards Australia (2004). *AS5100.6-2004 Bridge design, Part 6: Steel and composite construction*. Standards Australia International, Sydney, Australia.
- [16] Eurocode, 4 (2004). *Design of Composite Steel and Concrete Structures (BS EN 1994-1-1)*. British Standards Institution, London.
- [17] Wang, W. Da, Han, L.H. and Uy, B. (2008). “Experimental behaviour of steel reduced beam section to concrete-filled circular hollow section column connections”. *Journal of Constructional Steel Research*, 64(5), pp. 493–504.
- [18] Schneider, S.P. and Alostaz, Y.M. (1998). “Experimental Behavior of Connections to Concrete-Filled Steel Tubes”. *Journal of Constructional Steel Research*, 45(3), pp. 321–352
- [19] Fukumoto, T. and Morita, K. (2005), “Elastoplastic Behavior of Panel Zone in Steel Beam-to-Concrete Filled Steel Tube Column Moment Connections”. *Journal of Structural Engineering*, 131(12), pp. 1841–1853.

- [20] Rong, B., Yang, Z., Zhang, R., Feng, C., and Ma, X. (2019). “Postbuckling Shear Capacity of External Diaphragm Connections of CFST Structures”. *Journal of Structural Engineering*, 145(5), pp. 1–12
- [21] Zhang, D., Gao, S., and Gong, J. (2012). “Seismic behaviour of steel beam to circular CFST column assemblies with external diaphragms”. *Journal of Constructional Steel Research*, 76, pp. 155–166.
- [22] ABAQUS (2017). ABAQUS Theory and User’s manuals. Dassault systems, USA.
- [23] Han, L.H., Wang, W. Da., and Zhao, X.L. (2008). “Behaviour of steel beam to concrete-filled SHS column frames: Finite element model and verifications”. *Engineering Structures*, 30(6), pp. 1647–1658.
- [24] Zhang, Y.F., Zhao, J.H., and Cai, C.S. (2012). “Seismic behavior of ring beam joints between concrete-filled twin steel tubes columns and reinforced concrete beams”. *Engineering Structures*, 39, pp. 1–10.
- [25] Li, W., and Han, L.H. (2011). “Seismic performance of CFST column to steel beam joints with RC slab: Analysis”. *Journal of Constructional Steel Research*, 67(1), pp. 127–139.
- [26] Bhartiya, R., Sahoo, D.R., and Verma, A. (2021). “Modified damaged plasticity and variable confinement modelling of rectangular CFT columns”. *Journal of Constructional Steel Research*, 176.
- [27] Tao, Z., Wang, Z., and Yu, Q. (2013). “Finite element modelling of concrete-filled steel stub columns under axial compression”. *Journal of Constructional Steel Research*, 89, pp. 121–131.
- [28] Lubliner, J., Oliver, J., Oller, S., and Onate, E. (1989). “A plastic-damage model for concrete”. *International Journal Solids Structures*, 25(3), pp. 299–326.
- [29] Lee, J., and Fenves, G.L. (1998), “Plastic-Damage Model for Cyclic Loading of Concrete Structures”. *Journal of Engineering Mechanics*, 124(8), pp. 892–900.
- [30] ACI-318-14 (2014). *Building code requirements for structural concrete: (ACI 318-14); and commentary (ACI 318R-14)*. ACI. Farmington Hills.
- [31] CEB-FIP (1993). *CEB-FIB model code 1990: Design code*. Thomas Telford, London, p. 462.
- [32] Genikomsou, A.S., and Polak, M.A. (2015). “Finite element analysis of punching shear of concrete slabs using damaged plasticity model in ABAQUS”. *Engineering Structures*, 98, pp. 38–48.